

ARTICLE

## Design optimization of microfluidic-based solvent extraction systems for radionuclides detection

M. Pineda<sup>a</sup>, D. Tsaoulidis<sup>b</sup>, P. I. O. Filho<sup>a</sup>, T. Tsukahara<sup>c</sup>, P. Angeli<sup>d</sup>, and E. S. Fraga<sup>a</sup>

<sup>a</sup>Sargent Centre for Process Systems Engineering, Department of Chemical Engineering, University College London, London WC1E 6BT, UK; <sup>b</sup>Department of Chemical and Process Engineering, University of Surrey, Guildford GU2 7XH, UK; <sup>c</sup>Laboratory for Advanced Nuclear Energy, Tokyo Tech, Tokyo 2-12-1-N1-6 O-okayama, Meguro-ku, Japan; <sup>d</sup>ThAMeS Multiphase. Department of Chemical Engineering, University College London, London WC1E 6BT, UK

### ARTICLE HISTORY

Compiled September 16, 2021

### ABSTRACT

The development of reliable and fast automated methodologies to detect and identify radionuclides during the decommissioning of nuclear power plants is of paramount importance. In this regard, process flowsheeting and computational simulations are useful tools to aid the design and testing of these advanced detection technologies. We implement an optimization based design procedure for the design of continuous analysis systems based on microfluidic solvent extraction and on-line measurement to detect radionuclides in nuclear waste. The optimization of such detection systems is treated as a design under uncertainty problem. The systems are based on thermal lens microscopy as the detection instrument. We demonstrate our approach on a flowsheet for the detection of trivalent lanthanides in organic and aqueous solutions. We highlight the importance of using computer-aided optimization based procedures to design microsystems comprising several chemical operations and their coupling with the detection step. It constitutes a proof of concept and a first step towards robust optimization based modelling approaches for the design of microfluidic lab-on-a-chip platforms for the detection of radionuclides in nuclear waste.

### KEYWORDS

microdevices; radionuclides; solvent extraction; plug flow; detector design; stochastic optimization; design under uncertainty; thermal lens microscopy

## 1. Introduction

Decommissioning nuclear power plants is a long-term and costly endeavour. In the process of decommissioning the Fukushima Dai-chi Nuclear Power Plants, a large amount of radioactive waste, such as fuel debris, structural materials, rubble, soil, and adsorbents for treating contaminated water, has been generated. This waste poses many issues concerning nuclear cleanup, disposal and storage. Analysis of radionuclides is thus essential for realising efficient and safe treatment and disposal of this waste. However, fast and sensitive sensor systems are required for proper monitoring and

assessment.

A number of analytical techniques, based on the combination of chemical operations and large detection instruments such as inductively coupled plasma mass spectrometry (ICP-MS) and radiation spectrometry, have been applied to the analysis of decommissioning waste, such as that generated as a result of the Fukushima accident [1,2]. They have been recognized as superior analytical methods but have some disadvantages, e.g. they involve time consuming chemical operations (> hours), they require large sample volumes (> milliliter), and they produce secondary wastes (mL to L) and radiation toxicities. To overcome the disadvantages, novel methods such as laser resonance ionization and capillary electrophoresis have also been applied to the analysis of decommissioning wastes [3,4]. They realize highly sensitive detection for trace amounts of target elements, but are unsatisfactory due to the long-time measurement, limitation of sample properties (fluorescent reagent, pH range, aqueous solution, etc), requirement of large/expensive instruments, and bulk-scale pretreatment of samples using extraction, acidic eluents, and adsorbent resin. Therefore, simpler, faster, and less expensive analytical methods for detection of radionuclides would be desirable. In this context, computer simulations and optimization based design techniques are useful tools that can aid in the design and testing of process flow structures for radionuclides detection methods. We propose a methodology based on such methods for the generation of designs of analytic systems for radionuclides detection by means of microfluidic solvent extraction ( $\mu$ SE) coupled to thermal lens microscopy (TLM) as the detection instrument [5,6]. The reason is that the  $\mu$ SE/TLM device makes possible to in-situ detect trace elements in both aqueous and organic solvents, namely, it can identify accurately the microscale extraction pathway on-site and in real-time. A performance comparison of four analysis techniques with the  $\mu$ SE/TLM approach is presented in Table 1.

**Table 1.** Comparison of different analysis techniques.

	Laser resonance ionization	ICP-MS	Radiation spectroscopy	Capillary electrophoresis	$\mu$ SE/TLM (This work)
Analysis time	30 min	hours	hours	min ~	sec ~ min
Sensitivity	ppb ~ ppm	ppt	ppb ~ ppm	ppb ~ ppm	ppt ~ ppb
Sample volume	Solid	mL ~	mL ~	mL ~	pL ~ mL

Microfluidic systems, comprising channels with characteristic dimensions in the micrometre scale, have revolutionised chemical analysis where a separation method (e.g. solvent extraction) is commonly used as a tool to help the characterisation of a desired material [6–9]. In microchannels, transport resistances are reduced and heat and mass transfer rates intensified. Concentration and temperature fields become uniform rapidly and can therefore be more easily controlled. High conversion and selectivity may be achieved in these microsystems, leading to reduced waste and shorter residence times. Flow patterns can be established that increase the transport rates and interfacial area while facilitating the separation of phases at the end of the microchannels. The well defined flow patterns and the laminar flow conditions allow precise modelling and characterisation of such units. Plug flow, in particular with elongated drops of one phase flowing within the other, results in large interfacial areas, while circulation patterns in both phases intensify the mixing and exchange of mass transfer. The mass

transfer coefficients during plug flow are typically larger than in conventional contactors [10,11]. Microsystems are also attractive due to their ability to integrate series of fast chemical operational steps on small chips.

Microsystems have proved to be suitable for the solvent extraction and separation of radionuclides with very small volumes [12–16]. However, they typically lack the highly sensitive detectors needed for the online characterisation of the extracted and isolated components [17–19]. In this regard, TLM offers many advantages [20–22]. TLM uses laser microscopy based on the thermal lens effect (TLE) [23]. It is sensitive to analytes in liquids, appropriate for *in situ* analysis in microscopic space, and typically exhibits a very low limit of detection (LOD). TLM has already been used to investigate experimentally the parallel flow microfluidic-based solvent extraction of U(VI) from a HNO<sub>3</sub> solution by tributyl phosphate (TBP) in n-dodecane (n-DD) solvent [24]. In this case, the LOD value of the TLM apparatus for the U(VI) samples in both the aqueous and organic phases was determined to be approximately 10<sup>-4</sup> M. As a photothermal technique, TLM detection allows ultrasensitive detection of non-fluorescent analytes. Even in metal ions in a microchannel, concentration ranges less than micro molar have been successfully detected by means of TLM. Such detection sensitivity is much greater than UV-Vis spectrophotometry (milli molar level) [21,25]. As other methods, fluorescence spectrometry has been considered as effective detection tool; however fluorescent reagents are required while the aqueous solution properties, in particular, solution pH and the detectable analytes are strictly limited. Some researchers have developed microfluidic devices coupled with mass spectrometry for the determination of radionuclides [18]. However, strict microflow control is required to inhibit contamination of organic solvent into the aqueous phase, resulting in extremely narrow micro-extraction conditions. In addition, since certain solution conditions are required for applying mass spectrometry, e.g., use of only aqueous phase, acidity control, and back extraction from organic phase to aqueous phase, the techniques is less versatile than the  $\mu$ SE/TLM device. Accordingly, we have adopted the  $\mu$ SE/TLM approach as the most suitable one.

The TLE photothermal phenomenon is induced by coaxial beams comprising an excitation beam and a probe beam. The wavelength of the excitation beam is selected to coincide with an absorption band of the radionuclide to be detected. The wavelength of the probe beam is chosen so that the sample solution has no absorption. When the radionuclides in the confocal region absorb the excitation beam, they emit heat via radiationless processes. The temperature around the confocal region increases, and the refractive index decreases because of the heat. The laser intensity profile is nearly a Gaussian distribution, and so is the heat source distribution. The refractive index distribution becomes also a nearly Gaussian distribution and acts as a concave lens.

The selectivity of TLM is not necessarily sufficient because the presence of more than one radionuclide in the sample affects the detection of individual radionuclides. The sensitivity of the TLE, which is measured by the probe beam, is proportional to the quantity of emitted heat and therefore to the number of radionuclides in the confocal region. Thus, the heat emitted from different radionuclides could make them indistinguishable from one another.

Combining TLM with a microfluidic-based solvent extraction system may address the issue of selectivity by enabling the isolation of the target radionuclides. This combination enables online detection with small sample volumes and reduces waste and operating costs. Thus, the efficient isolation and purification of the radionuclides present in the feed to the detector is a crucial aspect for the detection of specific radionuclides. This requires multiple processing steps and the design of the isolation and purification

system requires the identification of these steps.

In a typical separation process for the isolation and purification of radionuclides [26], when the acidic feed solution contains a single extractable radionuclide and it is desirable to recycle the solvent, *extraction* and *stripping* units are needed. The stripping step consists of washing the extracted radionuclide back into the acidic media from the solvent and the solvent is recycled. However, when two radionuclides are present, extraction and stripping are not capable of producing any one radionuclide in relatively pure form because the organic phase leaving the extracting unit will carry some of every radionuclide in it. In this case, a *scrubbing* unit is added. The scrubbing unit removes all but the most extractable radionuclide from the organic phase leaving the extraction unit. For every additional extractable radionuclide to be separated in more or less pure form, two additional units are required, one for stripping and the second for scrubbing.

In this paper, we present a model-based optimization methodology for the design of microfluidic separation processes which, together with an online detection tool such as TLM, would be suitable as  $\mu$ TAS for the detection of multiple radionuclides in samples. The identification of suitable designs for such detection systems is treated as a problem of *design under uncertainty* [27,28]. As a case study, a simplified process flow structure suitable for the detection of two trivalent lanthanides (e.g. neodymium and samarium) in organic and aqueous solutions is presented. The separation, quantification, and detection of lanthanides is challenging due to their similar chemical and physical properties [29,30]. The process flow structure implements a separation procedure combining both extraction and scrubbing steps. Each step is assumed to consist of a mixing zone, a circular microchannel with a well developed plug (segmented) flow pattern, and a phase separator. The modelling of the flow pattern and mass transfer within the microchannels is based on a short-cut kinetic mass balance model and a correlation for the overall volumetric mass transfer coefficient taken from the literature [11,16]. Steady state ideal plug flow conditions are assumed in the microchannels for the development of such a model. The model does not take into account the usually complicated mass transfer process along the mixing and phase separation zones. It is also assumed that the feed compositions for all species other than the radionuclides are significantly in excess and do not change through the steps of the process. The distribution coefficients of the radionuclides are constant and the same for the extraction and scrubbing steps.

The paper is organised as follows. In Sec. 2, we present the radiochemical system considered as a case study and the process flow structure for radionuclides detection with an overview of the corresponding process models required for model based design. In Sec. 3, we formulate the optimization problem for the design of a detector including the objective and constraints which define its performance. Results are discussed in Sec. 4. Finally, summary and conclusions, including both the advantages and the disadvantages of the methodology, are presented in Sec. 5.

In this paper, the following terms are used:

**system** to refer to the combination of the separation process with the detection instrument;

**process** the actual configuration of the processing steps which isolates the radionuclides; and,

**detector** the specific detection instrument, e.g. the TLM discussed above.

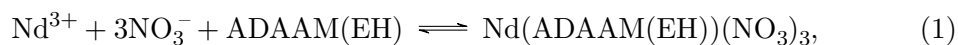
## 2. Case study

In this section, we introduce the specific radiochemical system considered in this work, the process flow structure for isolating the radionuclides, and the corresponding process models used for the optimization based design procedure described in Sec. 3.

### 2.1. Detection of lanthanides in organic and aqueous solutions

As a case study, we consider the detection of trivalent neodymium (Nd(III)) and trivalent samarium (Sm(III)) in organic and aqueous solutions, respectively. Detection using TLM is appropriate for this case, because lanthanides exhibit narrow adsorption bands [31]. In particular, since the absorbance at the maximum absorption wavelength is different for Nd(III) and Sm(III), excitation laser beams having different wavelength can be applied for TLM detection. Therefore, any interference effects of impurities such as other lanthanides and/or organic reagents on TLM signals can be eliminated, and the TLM can selectively detect target Nd(III) or Sm(III) in the solution. We use 2-ethylhexyl diamide amine (ADDAAM(EH)) in n-dodecane (n-DD) as the organic solvent. ADDAAM(EH) is a common and efficient extractant with a simple structure, developed for the separation of Am(III) from Eu(III) [32]. It exhibits high solubility in diluents like n-DD and has also been tested for the mutual separation of Am(III) and Cm(III) in acidic media by using multistage countercurrent mixer-settler extractors [33].

Equilibrium batch experiments indicate that the extraction mechanism of Nd(III) and Sm(III) from acidic aqueous solutions (as nuclear waste is often processed with acid solutions) into an organic solution is as follows:



and

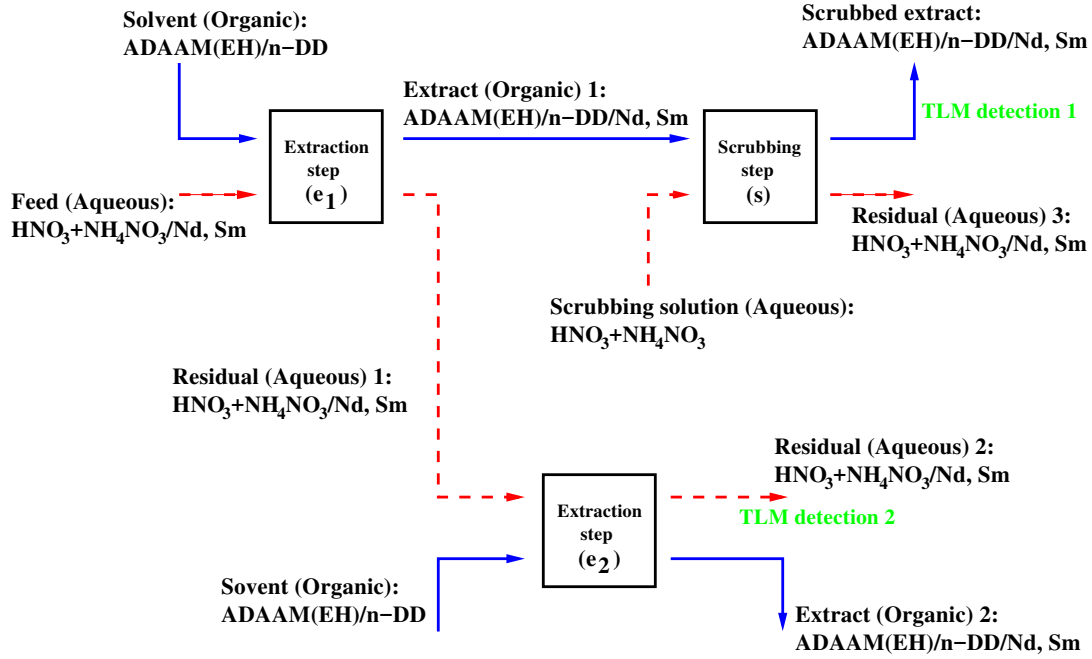


where  $\text{Nd}(\text{ADAAM})(\text{NO}_3)_3$  and  $\text{Sm}(\text{ADAAM})(\text{NO}_3)_3$  are extractable metal-organic complexes and  $\text{NO}_3^-$  are nitrates in the aqueous solution. Experimental reports show also that Nd(III) is more extractable than Sm(III): the distribution coefficient, which describes the concentration of the radionuclide in the organic phase to the concentration in the aqueous phase at equilibrium [26], of Nd(III) is greater than the distribution coefficient of Sm(III) [34]. In the following section, a process structure, or *flowsheet*, for isolating the desired radionuclides is proposed which exploits this difference in distribution coefficients. Isolating the radionuclides will enable detection of each one separately with a quantifiable degree of confidence.

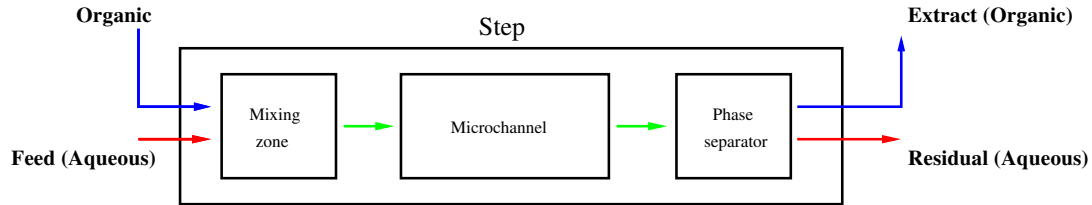
### 2.2. Flowsheet for the detection of radionuclides

Fig. 1 presents a process flowsheet suitable for the isolation and subsequent detection of two independent radionuclides that may be present in an acidic sample. The flowsheet consists of a series of steps, combining extraction and scrubbing. The structure of each step is presented in Fig. 2.

The presence and amounts of the radionuclides in the feed sample are unknown.



**Figure 1.** A process flowsheet for the detection of two radionuclides using thermal lens microscopy. Each step, indicated by a square block in the diagram, consists of a mixing zone, a circular microchannel with a well defined segmented flow pattern, and a two phase separator (see Fig. 2 for a detailed representation of a step). The TLM detection of Nd(III) occurs on the organic scrubbed extract output (top right output of the process, in blue) and the detection of Sm(III) takes place on the second aqueous residual output (output of the  $e_2$  extraction step, red dashed line). We use the symbols Nd and Sm to denote trivalent neodymium and trivalent samarium, respectively.



**Figure 2.** Schematic of a solvent extraction step. The aqueous and organic solutions come into contact in the mixing zone (e.g. a T-junction). Then, a well defined flow pattern emerges along a circular microchannel. Finally, the two phases are separated by a specific phase separator method which can take advantage of the difference in wettability between the two phases.

The aim of the process is to isolate radionuclides which may be present sufficiently to detect their presence using TLM. The process implements a separation procedure combining both extraction and scrubbing steps. This suggested process does not consider recycling of the solvent, a feature of large scale reprocessing plants which deal with much larger volumes [35] but which is not necessary for a micro-analytic detection system. As a result, a stripping step to recover the solvent is not considered.

Each step (Fig. 2) consists of a mixing zone, a circular microchannel with a well developed segmented flow pattern, and a phase separator. We consider segmented flow patterns (see Fig. 3) because they enhance two-phase mixing and their hydrodynamic properties may be more easily controlled to improve mass transfer [14,15]. Typically,

the phase separation at the end of the microchannel extractor is achieved by exploiting the differences in surface wettability between the aqueous and organic phases [12,13].

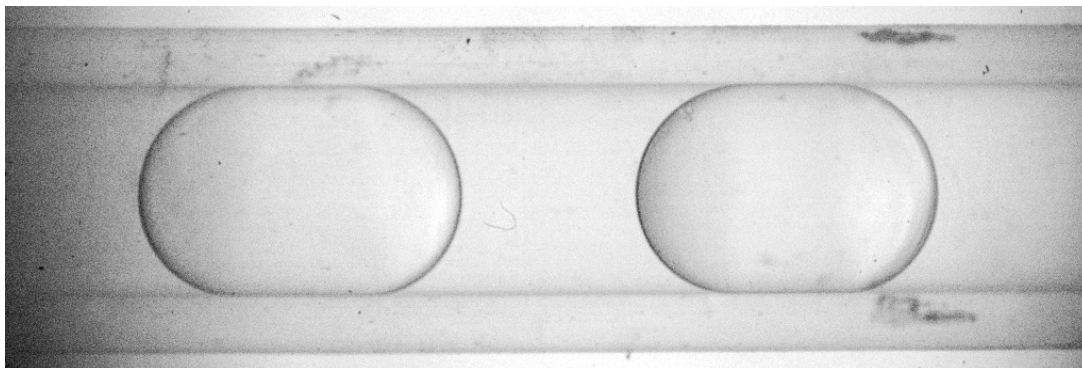


**Figure 3.** Photograph of segmented flow pattern achieved in a microchannel, courtesy Dr Haoyu Wang, UCL. We consider a segmented flow pattern because it combines improved radial mixing due to the circulation patterns that are established within each phase [36], with large interfacial areas. The microchannel is made of polytetrafluoroethylene (PTFE). However, the same pattern also forms in channels constructed from glass or other materials.

The feed, for the process in Fig. 1, is an aqueous solution of  $\text{HNO}_3$  and  $\text{NH}_4\text{NO}_3$  containing some unknown, possibly zero, amounts of Nd(III) and Sm(III). The feed is brought in contact, in the mixing zone of the first extraction step,  $e_1$ , with an organic solution composed of the extractant ADAAM(EH) in n-DD. The extraction step  $e_1$  occurs in a hydrophobic circular microchannel where dispersed plugs (elongated drops) of the aqueous phase are formed inside the continuous organic phase. Fig. 3 illustrates the well developed segmented flow regime that may be achieved in a circular microchannel. In this first step, mass transfer takes place from the aqueous phase to the organic phase, with Nd(III) being preferentially transferred.

At the end of the microchannel, a phase separator is used to transfer the aqueous stream to a side hydrophilic microchannel forming the first residual (aqueous) stream as one of the two outputs of this first step. This residual stream enters a second extraction step,  $e_2$ , where it is brought into contact with a fresh organic solution of ADAAM(EH) in n-DD. In this step, the extraction process also occurs inside a hydrophobic circular microchannel under segmented flow conditions. The aim of this step is to remove any Nd(III) present in the feed to this step. Any such amount of Nd(III) will leave in the organic phase. If Sm(III) were present in the feed stream to the second step, most of it will remain in the aqueous phase and the TLM will be used to detect its presence in the aqueous output of step  $e_2$ .

The organic extract from the first extraction step is fed to a scrubbing step (denoted as  $s$  in Fig. 1). The role of this step is to scrub or remove the less extractable Sm(III) from the organic phase, leaving most of the Nd(III) in the organic phase. In this purification step, the organic extract is brought in contact with a pure  $\text{HNO}_3$  and  $\text{NH}_4\text{NO}_3$  scrubbing aqueous solution in a new hydrophobic circular microchannel which also forms dispersed plugs of the scrubbing solution. Finally, the organic stream is separated from the aqueous stream via a side hydrophobic microchannel, leading to an output suitable for detection of Nd(III) in the scrubbed extract using TLM. During the scrubbing process, small amounts of Nd(III) are also transferred to the aqueous phase.

The design of this process entails the sizing of each step and determining the

amounts of other feeds to the process to enable the suitable separation of the unknown quantities of radionuclides in the feed for detection in the appropriate output streams. The sizes of the channels and the flow rates are the *design variables* for an optimization based design method. The relevant TLM property for detection is the limit of detection (LOD) of each radionuclide. The LOD of a radionuclide in a sample is the minimum concentration which yields an analytical signal, a signal which is significantly different to that of the blank sample [37]. Concentrations below this limit may not be detected. The LOD imposes constraints on the performance achievable in the design of the system.

To determine suitable specific properties of a design for this process, we propose the use of model based optimization. The following section presents the mathematical models of the extraction and scrubbing steps in the process. The models describe the behaviour of the process for any suitable combination of values for the design variables and are used to predict the detection capabilities of the resulting system.

### 2.3. Process modelling

Modelling solvent extraction of lanthanides in microchannels has been previously addressed using simplified computational fluid dynamics [38,39]. Incorporating such models into an optimization based design procedure may lead to computationally expensive or even intractable problems. Instead, a simpler model, which incorporates overall mass transfer coefficients derived from dimensional analysis and experiments data [11,14,15,22], has been implemented. This approach has been used previously for large scale separation process design for reprocessing [16,35].

The model takes into account mass transfer within the well developed segmented, i.e. plug, flow pattern of the circular microchannel (see Fig. 3). During plug flow, axial mixing is limited and radial mixing is improved [36]. Therefore, the circular microchannel can be modelled as an ideal plug flow reactor [16,40].

Then, the concentration of each radionuclide in the aqueous (dispersed) phase ( $a$ ) in each step evolves according to

$$\nu_{a,j} \frac{d}{dx} C_{a,i,j}(x) = -K_j [C_{a,i,j}(x) - C_{a,i,j}^*(x)], \quad (3)$$

and the concentration in the organic continuous phase ( $o$ ) as

$$\frac{d}{dx} C_{o,i,j}(x) = -q_j \frac{d}{dx} C_{a,i,j}(x), \quad (4)$$

where  $i \in \{Nd, Sm\}$  is the subscript which refers to the individual radionuclides,  $j \in \{e_1, e_2, s\}$  is the subscript that refers to the processing step (as labelled in Fig. 1),  $q_j = \frac{\dot{Q}_{a,j}}{\dot{Q}_{o,j}}$  is the ratio of the volumetric flow rate of the aqueous phase to that of the organic phase for each step, and  $\nu_{a,j} = \dot{Q}_{a,j}/A_j$  is the superficial velocity of the aqueous phase.  $A_j = \pi D_j^2/4$  is the transversal area of the circular microchannels where  $D_j$  is the diameter of the channel in the  $j$ -th processing step.

In each step, let  $x \in [0, L_j]$  denote the position along the channel, where  $L_j$  is the length of the channel in the  $j$ -th step. The term  $C_{a,i,j}^*(x) = C_{o,i,j}(x)/\alpha_i$  is the so called equilibrium line and  $\alpha_i$  is the distribution coefficient [26]. In this work, the concentrations of the radionuclides will be small so the distribution coefficients are

taken to be constant along the microchannels.

For the overall volumetric mass transfer coefficient,  $K_j$ , the product between the mass transfer coefficient and interfacial area, we consider the correlation suggested by Kashid et al. [11],

$$K_j = \left( \frac{\dot{Q}_{a,j} + \dot{Q}_{o,j}}{A_j} \right) \left( \frac{Ca^{-0.09} Re^{-0.09}}{L_j} \right) \left( \frac{D_j}{L_j} \right)^{-0.1}. \quad (5)$$

This correlation is an average value derived from a dimensional analysis of experimental data from polytetrafluoroethylene (PTFE) microchannels under segmented flows. It has shown good agreement with data from experiments on the microfluidic-based solvent extraction of U(VI) and Eu(III) [14,15]. It is important to mention, however, that PTFE is a sensitive type of plastic and not suitable for applications involving long exposure to radiation. An actual  $\mu$ TAS system will preferably be made from glass or metallic materials [5,41–44]. In any case, once segmented flow is established, the channel material is not relevant in terms of performance. The Reynolds ( $Re$ ) and Capillary ( $Ca$ ) numbers are calculated following Kashid et al. [11].

### 3. Design optimization for detection

Designing a detector for the presence of radionuclides requires identifying a design of a suitable process to isolate the radionuclides to be detected. This is similar to the design of an intensified operation for separation of radionuclides for reprocessing although the objectives are different. In reprocessing, the goal is to extract as much of the desired radionuclides as possible, usually also with the highest purity possible. In a detector, the goal is to extract the individual radionuclides sufficiently to identify their presence, or to note that they are absent. When there may be more than one radionuclide present, the design of the detector also imposes purity requirements. Both reprocessing and detection therefore share aspects of design goals.

However, in the case of reprocessing, the feed to the process is usually well characterised [26,35]. For a detector, although certain information about the feed would have to be known to motivate its analysis, such a feed is usually not well characterised. The aim of the system is to determine information about the unknown composition of the feed. Specifically, the purpose of an analysis system is to identify the presence or absence of specific radionuclides in the feed to the system. Generating the design of such a system can therefore be considered to be a problem of *design under uncertainty* [27,28].

An analysis system will be characterised by its sensitivity, its limit of detection. This limit will be based on not only the limits inherent in the specific detector used but also the performance of the extraction process in isolation the radionuclides. In the case presented here, the detection is provided by thermal lens microscopy and each radionuclide will have a specific  $LOD_i$ , using the notation introduced in Section 2.3. The process itself will have a limit on the purity achievable through extraction as a function of the actual design and the distribution coefficients of the individual radionuclides. Therefore, the sensitivity of the analysis system will be lower than that of the detector due to the combination of the process performance and the detector's own limits.

The aim in the design of a detection system, then, is to identify a design which has

the best sensitivity or, in other words, the lowest limit of detection. A design is defined by the design variables which, in the case of the process structure shown in Fig. 1, are the lengths and diameters of the channels for each step and the flow rate ratios between the aqueous and organic feeds to each step.

As the feed is unknown, an individual design is evaluated by considering a large number of different feed compositions, with concentrations of the radionuclides chosen randomly and uniformly from a range of concentration values for each radionuclide that could be present. For each feed composition sample, the process design is simulated using the model described in Section 2.3 and the ability to detect the presence of the radionuclides is evaluated. This evaluation consists of determining whether the TLM system would be able to detect the individual radionuclide in the respective stream (as shown in Fig. 1 and indicated as *TLM detection* in green).

If the process simulated identifies the presence of each radionuclide when present in the feed, above the limit of detection for the device, or correspondingly the absence of that radionuclide, the process is deemed to be *feasible*. If, however, the device fails to detect the presence of a radionuclide when it was present in the feed, for any of the random feed samples, the process is not feasible and we state that this process results in a *false negative* result. Alternatively, if the detection system would indicate the presence of a radionuclide when in fact that radionuclide was not present in the feed, this process is also deemed *infeasible* and we state that the process with the particular feed results in a *false positive* result.

False negatives are deemed to be significantly worse than false positives. The former can lead to material being assessed as safe (from the point of view of radioactivity) when it might not be; the latter, however, may simply require more processing and effort but does not necessarily impact on safety. The relative importance of these outcomes will be used below in the definition of a multi-objective optimization variation for the design of the process.

### 3.1. The optimization problem

As noted above, the limit of detection for the system is a function of the extraction performance of the process and the actual limits imposed by the detection method (TLM in our case). We define  $\phi$  as a measure of the performance of the system.  $\phi$  is a measure of the limit of detection for the system relative to the individual detector limits of detection. A feasible design will be one which will be able to detect the presence of each radionuclide if present in the feed to the detection system with a concentration of at least  $\phi \times \text{LOD}_i$  and which may indicate absence of that radionuclide if present in the feed with a concentration no more than  $\phi \times \text{LOD}_i$ . The smaller the value of  $\phi$ , the less of a penalty is imposed by the process on the performance of the system. Since the system cannot improve on the limit imposed by the detector,  $\phi$  must be greater than 1. The objective of the optimization procedure will then be to find the smallest value of  $\phi$  for which a design is feasible, i.e. has no false negative or false positive readings:

$$\begin{aligned} & \min_{d \in \mathcal{D}} \phi & (6) \\ \text{subject to} & \quad n_f(d, \phi) \leq 0 \\ & \quad n_p(d, \phi) \leq 0 \end{aligned}$$

where  $n_f(d, \phi)$  is the number of false negative readings found for the given design and  $n_p(d, \phi)$  is the number of false positive readings found. A design, represented by the values of the design variables,  $d$ , is simulated for each of the different feed compositions sampled from the space of all possible feed compositions; the number of false negative and positive readings is the sum of how many feed samples result in false readings. This approach of sample based evaluation is similar to that developed for an industrial process scale-up problem involving aerosols with probability distributions for describing the feed [45]. The result of solving this optimization problem will be the design,  $d^*$ , which has the smallest value of  $\phi$  possible and which results in no false readings.

The calculation of the false negatives and positives can be summarised mathematically as

$$n_f(d, \phi) = \sum_{s \in \mathcal{S}} \sum_{i \in \{\text{Nd}, \text{Sm}\}} \begin{cases} 1 & C_{i,0} > \phi \times \text{LOD}_i \wedge C_i(d) < \text{LOD}_i \\ 0 & \text{otherwise} \end{cases} \quad (7)$$

$$n_p(d, \phi) = \sum_{s \in \mathcal{S}} \sum_{i \in \{\text{Nd}, \text{Sm}\}} \begin{cases} 1 & C_{i,0} < \text{LOD}_i \wedge C_i(d) > \text{LOD}_i \\ 0 & \text{otherwise} \end{cases} \quad (8)$$

where  $\wedge$  is the logical “and” operator.  $\mathcal{S}$  is the set of sample feed compositions to consider, generated randomly,  $C_{i,0}$  is the concentration of radionuclide  $i$  in the feed to the detector, and  $C_i(d)$  represents the concentration of the radionuclide at the point of detection in the process for the design represented by  $d$ . False negatives, in terms of the system as a whole, occur when the feed has a concentration greater than  $\phi$  multiplied by the detector’s LOD but the concentration at the detection point is less than that LOD. False positives occur when the feed has a concentration lower than the LOD yet the concentration at the detection point exceeds that limit. The definition of false positive cases could have included the value of  $\phi$ ; by not doing so, we have made the condition less strict, noting the false positive cases are not as concerning as false negative cases.

At first glance, it would seem not possible to generate false positive readings but these may occur for two reasons:

- (1) the concentration depends not only on the amount of the radionuclide but also on the volumetric flow rate of the stream. One of the design variables is implicitly the flow rate of solvent introduced for the extraction. A low flowrate could lead to a higher concentration at the point of detection by extracting a certain amount of the radionuclide into a low flow rate stream.
- (2) the detection mechanism may not be able to differentiate between the different radionuclides. This is true for TLM. There may be overlap in the detection and this will be addressed below.

### 3.2. The optimization method

The optimization problem (equation 6) is a nonlinear dynamic optimization problem with continuous design variables. This type of problem can be solved in a number of ways. One approach is to discretize the differential equations in the model. The result is then an algebraic model which would be classed as a nonlinear programming (NLP) optimization problem. NLP problems which can be solved with a wide range of tools.

However, the discretization leads to a large problem which may pose computational challenges. Instead, we propose the use of a *black box* optimization procedure that can use the model as defined above directly, in the form of differential equations.

The specific procedure is Fresa [46], a nature inspired plant propagation algorithm [47] which has been previously used successfully for nonlinear dynamic optimization problems [48]. Fresa is a population based evolutionary search procedure. It uses stochastic selection and solution transformations based on the fitness of the individual designs in the population.

Fresa is implemented in the Julia language [49] with the stochastic modelling provided by an uncertainty modelling framework [50]. Julia enables the use of parallel processing which allows the summations in equations 7 and 8 to be distributed over multiple cores. We have used a 24 core desktop computer system for the results presented below; details of this system are given below.

#### 4. Results for the design of an analysis system

The optimization problem described in the previous section is solved using the Fresa optimization solver for the process structure described in Section 2.3. The actual problem requires the specification of the feed to the process. The feed composition for all species other than the radionuclides is fixed: 0.1 M HNO<sub>3</sub>, 3.0 M NH<sub>4</sub>NO<sub>3</sub> for the aqueous feeds, also containing the radionuclides with uncertain concentrations, and 0.5 M ADAAM(EH) in n-DD for the organic feeds [34]. It is assumed that these concentrations are significantly in excess in comparison with the concentrations of the radionuclides and so they will be taken as constant throughout the steps of the process. The concentrations of the two radionuclides will vary, as noted in the previous section. The interfacial tension, densities, and viscosities used to calculate the Reynolds and Capillary numbers for the process are given in Table 2 for the two phases.

**Table 2.** Fluid properties for the case study [51].  $\gamma$  represents the interfacial tension between the two phases (aqueous and organic).

Properties	Phase		Units
	Organic	Aqueous	Units
Interfacial tension, $\gamma$	0.01		N m <sup>-1</sup>
Viscosity, $\mu$	0.0023	0.001	kg m <sup>-1</sup> s <sup>-1</sup>
Density, $\rho$	844	997	kg m <sup>-3</sup>

For the  $\mu$ TAS system using TLM for the detection of the individual radionuclides, the limit of detection for Nd(III) and Sm(III), under the conditions considered, could range from 10<sup>-4</sup> M to 10<sup>-5</sup> M. The LOD of Nd(III) and Sm(III), based on their absorption spectrum [31], are assumed to be LOD<sub>Nd</sub> = 10<sup>-4</sup> M and LOD<sub>Sm</sub> = 10<sup>-5</sup> M, respectively [24]. The distribution coefficients of Nd(III) and Sm(III) in the extraction and scrubbing steps for those conditions are  $\alpha_{Nd} = 3.7$  and  $\alpha_{Sm} = 0.3$  [34]. The volumetric flow rate of the feed to the process is fixed at  $\dot{Q}_{a,e_1} = 1.3 \times 10^{-8}$  m<sup>3</sup> s<sup>-1</sup>; with this volumetric flow rate, a segmented flow pattern is observed experimentally for the fluid properties in Table 2 and with values of the process design variables within the bounds given in Table 3. Any variation of  $q_{e_1}$  requires the manipulation of  $\dot{Q}_{o,e_1}$ , the flow rate of the organic feed. Similarly, variations of  $q_{e_2}$  ( $q_s$ ) occur only if  $\dot{Q}_{o,e_2}$  ( $\dot{Q}_{a,s}$ ) vary.

For any given process design,  $n_s$  samples will be generated. The 2-dimensional

**Table 3.** Design variables and their domains for the search with  $j \in \{e_1, s, e_2\}$  [14,15,24]. All processing steps will have the same microchannel diameter.

Variable	Description	Domain	Units
$D$	Channel diameter	[0.0005, 0.001]	m
$L_j$	Channel length	[0.05, 0.4]	m
$q_j$	Ratio of aqueous to organic flow rates	[0.5, 2.0]	

sampling space is defined by the intervals of possible initial concentrations of each of the radionuclides:  $C_{i,0} \in [0, 0.001]$  M for  $i \in \{\text{Nd}, \text{Sm}\}$ . Each design considered will be evaluated for each of the samples, i.e. each different feed composition. The value of  $n_s$  will be  $10^5$  unless otherwise stated.

For the application of the Fresa optimization solver, default values of the plant propagation algorithm parameters have been used. The population size is  $n_{\text{pop}} = 5$  and  $n_{\text{gen}} = 40$  generations are performed. Fresa generates, on average, 2.5 new solutions for each member of the population at each generation. The settings for Fresa lead typically to the evaluation of just over 500 process designs in the search. Each of these designs is simulated  $n_s$  times so that on the order of 50 million simulations are performed during the search. To cater for the small concentrations considered potentially for the radionuclides, the relative tolerance for the differential equation solver, provided by the `DifferentialEquations.jl` package,<sup>1</sup> is  $10^{-9}$  which leads to a significant increase in the computation required for each simulation.

A system with 24 3.00 GHz Intel Xeon E5-2687 cores and 32 GB of RAM is used. On this system, the solution to the optimization problem, with the settings described above, takes a little over 1 hour of computation when taking advantage of the multiple cores by invoking the parallel computation feature in Fresa. Due to the stochastic nature of Fresa and the problem itself, the design problem is solved multiple times to determine whether the stochastic aspects affect the quality of designs obtained.

#### 4.1. Initial design

Fresa has been applied 10 times to the problem defined in Equation 6, with the settings described above. In all cases, the convergence of the population follows a profile similar to that shown in Fig. 4. A feasible solution, one for which there are no false readings for any of the feed composition samples, is found quickly (by the second generation in the case shown in Fig. 4) and then the value of  $\phi$  quickly decreases until it reaches a value close to the final best solution.

The stochastic nature of Fresa and, to some degree, the sampling of the feed composition mean that the solutions obtained in different attempts will differ slightly. This is evident in the value of  $\phi$  obtained and also the actual designs that correspond to the best solutions from the different runs. In terms of  $\phi$ , we obtain values with a mean of 1.71 and a standard deviation of 0.25. Given the approximations in the modelling and the stochastic nature of the method, we would conclude that a  $\mu$ TAS could be designed with a limit of detection which is twice the limits of the detector. For detection using TLM, this would mean a limit of detection for the system of  $2 \times 10^{-4}$  M for Nd and  $2 \times 10^{-5}$  M for Sm.

As the actual design obtained in each run may be different, Fig. 5 (presenting the outcome for the geometric design variables) and Fig. 6 (operating design variables) show the different designs obtained from 10 applications of Fresa to the design problem,

<sup>1</sup><https://github.com/SciML/DifferentialEquations.jl>

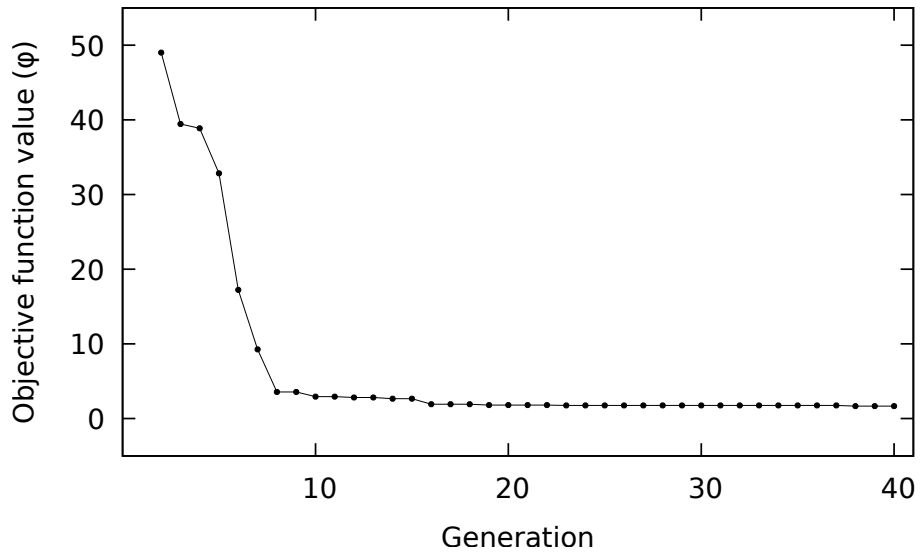


**Figure 4.** The evolution of the best solution in the population, starting from the first feasible solution found which is the second generation in this case. The lower bound on  $\phi$  is 1.0.

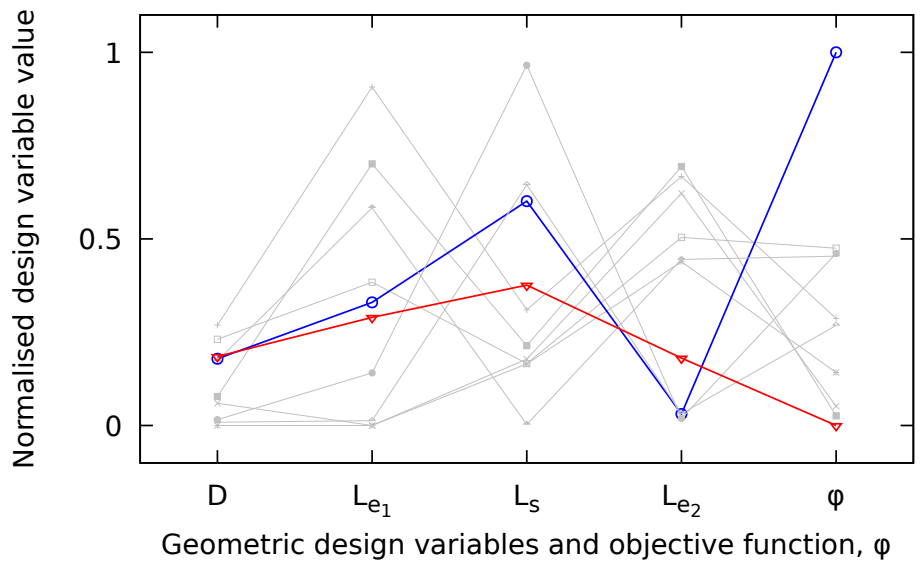


**Figure 5.** A parallel coordinate plot showing the values of the geometric design variables, normalised within their respective domains as given in Table 3, and the value of  $\phi$  obtained, normalised with respect to the minimum and maximum values obtained in 10 runs. Each poly-line represents a process design. The poly-line representing the design with the lowest value of  $\phi$  is highlighted in red with downward pointing triangles ( $\nabla$ ) and that with the highest value of  $\phi$  is highlighted in blue with open circles ( $\circ$ ).

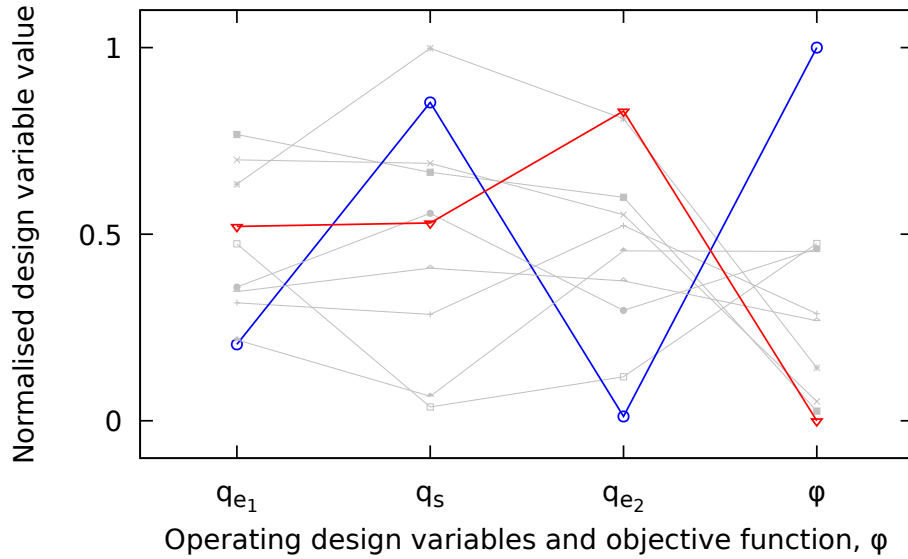


**Figure 6.** A parallel coordinate plot showing the values of the geometric design variables, normalised within their respective domains as given in Table 3, and the value of  $\phi$  obtained, normalised with respect to the minimum and maximum values obtained in 10 runs. Each poly-line represents a process design. The poly-line representing the design with the lowest value of  $\phi$  is highlighted in red with downward pointing triangles ( $\nabla$ ) and that with the highest value of  $\phi$  is highlighted in blue with open circles ( $\circ$ ).

**Table 4.** Values of the design variables for the best design, as highlighted in Fig. 5 and in Fig. 6, with value of  $\phi$  for the design.

Variable	Value	Units
$D$	0.59	mm
$L_{e_1}$	0.15	m
$L_s$	0.18	m
$L_{e_2}$	0.11	m
$q_{e_1}$	1.28	
$q_s$	1.29	
$q_{e_2}$	1.74	
$\phi$	1.45	

equation 6. The solution with the lowest value of  $\phi$  has been highlighted in the figures in red and the values for the design variable for this design can be found in the first row of Table 6 below, a table which summarises these and subsequent results. There is no clear pattern from the distribution of design variable values obtained. This indicates that the search space is likely multi-modal and that alternative designs are possible for the same design task with similar performance. However, it should be noted that the optimization problem defined (equation 6) considers only the value of  $\phi$  and the number of false readings in comparing alternative designs during the search. In process design more generally, economic considerations are often included in the optimization problem. This would typically lead to designs with more similar configurations. For the design of the process for the detection system, a second objective could be added that incorporates an element of cost or, in the case of a  $\mu$ TAS specifically, the space required on a microchip for efficient manufacture.

#### 4.2. Detection interference

The detection mechanism used may not be able to distinguish completely between different radionuclides. This is true of the thermal lens microscope used here where the presence of another radionuclide affects the detection of a given radionuclide. This may lead to false positive readings and we may wish to ensure the design of the detector takes this into consideration. We can do this by modifying the definition of false readings:

$$n_f(d, \phi) = \sum_{s \in \mathcal{S}} \sum_{i \in \{\text{Nd, Sm}\}} \begin{cases} 1 & C_{i,0} > \phi \text{LOD}_i \wedge C_i(d) + \delta C_k(d) < \text{LOD}_i \\ 0 & \text{otherwise} \end{cases} \quad (9)$$

$$n_p(d, \phi) = \sum_{s \in \mathcal{S}} \sum_{i \in \{\text{Nd, Sm}\}} \begin{cases} 1 & C_{i,0} < \text{LOD}_i \wedge C_i(d) + \delta C_k(d) > \text{LOD}_i \\ 0 & \text{otherwise} \end{cases} \quad (10)$$

where  $\delta \in [0.0, 1.0]$  is a measure of overlap in readings between the two radionuclides. A value of 0.0 means that the detection mechanism can distinguish perfectly between the two radionuclides involved; a value of 1.0 means they are indistinguishable from each other. In the equations above, the  $k$  subscript refers to the other radionuclide.

We consider solving the same design problem with values of  $\delta \in \{0.25, 0.50, 1.00\}$ . For  $\delta=0.25$ , we find that the detector limit of detection is now a little higher, i.e. less sensitive. Specifically, we generate designs with an average value of 2.60 with a standard deviation of 0.33. So, we would describe the  $\mu$ TAS designed as being suitable for radionuclide minimum concentrations of  $3 \times 10^{-4}$  M for Nd and  $3 \times 10^{-5}$  M for Sm.

The designs obtained are presented in Fig. 7 and Fig. 8, again using a parallel coordinate plot, with design variable values for the lowest  $\phi$  value given in Table 5. This time we see that the designs that take into account possible interference in the detection mechanism have some visible differences with the best solution found without taking this interference into account. In particular, the aqueous to organic flow rate ratios for the two extraction steps,  $e_1$  and  $e_2$  are higher than those found for the interference case. The concentration of Sm(III) at the point of detection decreases when the flow rate ratios of the extraction steps decrease, since more solvent is used. This compensates for the interference due to the presence of neodymium. Note also

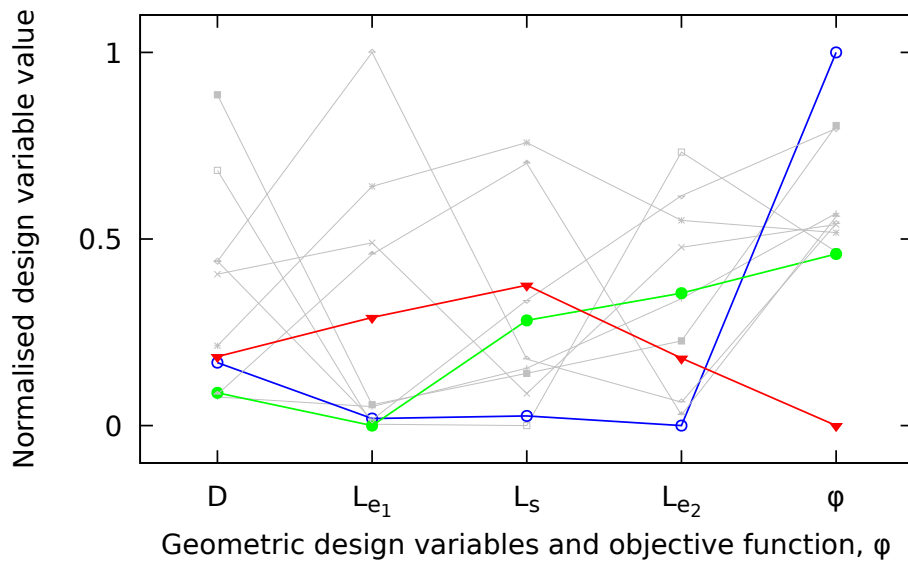


**Figure 7.** Parallel coordinate plot of the design variables when interference in detection is  $\delta = 0.25$ . The best design for this case is shown in green with filled circles ( $\bullet$ ) and least best outcome from the 10 runs is highlighted in blue with open circles ( $\circ$ ). For comparison, the original best design is also indicated, again in red, with filled downward pointing triangles ( $\blacktriangledown$ ).

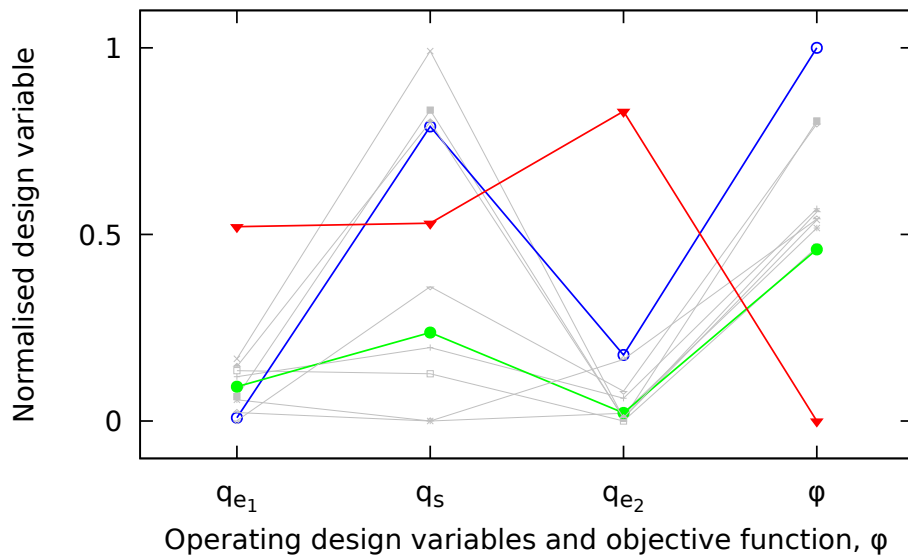


**Figure 8.** Parallel coordinate plot of the design variables when interference in detection is  $\delta = 0.25$ . The best design for this case is shown in green with filled downward pointing triangles ( $\blacktriangledown$ ) and the least best design obtained is shown in blue with open circles ( $\circ$ ). For comparison, the original best design is also indicated, again in red, with downward pointing triangles ( $\blacktriangledown$ ).

**Table 5.** Values of the design variables for the best design for a detection overlap of  $\delta=0.25$ , as highlighted in Fig. 7 and Fig. 8, with value of  $\phi$  for the design.

Variable	Value	Units
$D$	0.54	[mm]
$L_{e_1}$	0.05	[m]
$L_s$	0.15	[m]
$L_{e_2}$	0.17	[m]
$q_{e_1}$	0.64	
$q_s$	0.86	
$q_{e_2}$	0.53	
$\phi$	2.30	

that the optimum values of  $q_s$  are higher than  $q_{e_1}$ . This means that the organic to aqueous flow rate ratio in the scrubbing step is less than in the extraction step. This is usually not the case for scrubbing of loaded organic where typically a small amount of aqueous phase is contacted with a relatively larger amount of organic phase so that only the less extractable species is back-extracted from the organic phase to the aqueous phase while more extractable species are retained in the loaded organic. However, it is important to note that, for this system, separation is performed for the purpose of detection, i.e. identification of presence of components above some amount, and not purification.

From Fig. 8, what is also apparent is a correlation between the value of  $\phi$  obtained and the values of the ratios of the flow rates: as mentioned above, not only is  $q_s$  higher than  $q_{e_1}$ , and also higher than  $q_{e_2}$ , but also there appears to be a minimum value for each of these that leads to the best outcome. Increasing these flow rate ratios results in a less performant system.

For the other values of  $\delta$  considered, no feasible designs were found. All designs, regardless of  $\phi$  value (within the domain considered for this variable, i.e.  $\leq 100$ ), would generate false positive readings for some sample feed compositions. The interference between the two radionuclides require more isolation than is possible with the process structure considered. A better structure may be able to isolate the radionuclides; this is discussed in the next section in more detail. It should be noted, however, that because the adsorption peaks of both radionuclides are well separated, the level of interference expected would correspond to a value of  $\delta$  less than 0.25 [31].

In any case, false positive readings, although undesirable, do not pose any issue of safety. It may be worth exploring what designs might perform well even if they would lead to false positive readings.

### 4.3. Multi-objective design

The design problem has to be posed differently to enable us to consider what we have previously identified as infeasible designs. Fresa is able to solve multi-objective optimization problems so the original optimization problem is converted from a single objective problem with constraints to a bi-objective problem where the constraints have been transformed to a second objective:

$$\min_{d \in \mathcal{D}} z = \left[ \begin{array}{c} \phi \\ n_f + 10^{-3}n_p \end{array} \right] \quad (11)$$

where  $z$  is a the bicriteria objective function. The first objective is the limit of detection for the system,  $\phi$ , as before. The second objective is a combination of the number of false negatives,  $n_f$ , and false positives,  $n_p$ . As the presence of false negative readings poses safety issues, these are emphasised when compared with false positive readings. Ideally, we shall find solutions which have no false negatives, and minimal incidents of false positives, and we will be able to see how the system limit of detection trades-off with the number of false positives.

For the multi-objective problem, we change the parameters for the search procedure in Fresa:

- (1) the population size is now dynamic, with Fresa being able to adjust the population size between a minimum of 5 and a maximum of 20. Fresa will choose the population size to ensure that the set of non-dominated points, an approximation to the Pareto front, is less than half of the population, whenever possible given the bounds on the population size.
- (2) the number of generations is increased to 100 to cater for needing to generate a trade-off set rather than just one solution.

All other parameters remain the same. The change in settings results in an increase in the computational requirements. The problem, Eq. 11, now takes approximately 10 hours to solve, an increase consistent with the increase in population and the number of generations.

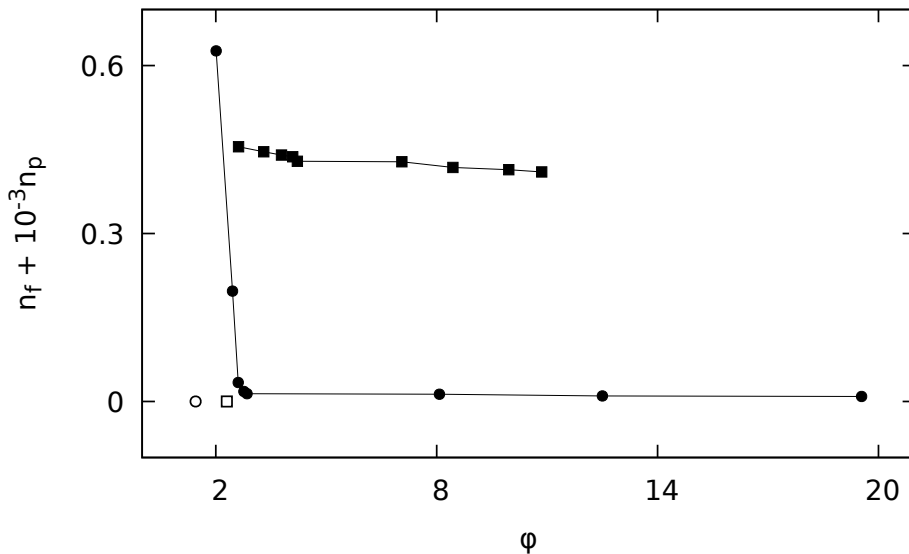


**Figure 9.** Sets of non-dominated points, showing the trade-off between number of false readings ( $n_f + 10^{-3}n_p$ ) and the system limit of detection,  $\phi$ , for the design of a detection system with different levels of interference in detection,  $\delta=0.5$  for graph with filled circles ( $\bullet$ ) and  $\delta=1.0$  for graph with filled squares ( $\blacksquare$ ). The lines connecting the points are simply for illustration and do not represent any actual design. The single points near the bottom left of the plot are for  $\delta=0.0$  with an open circle ( $\circ$ ) and  $\delta=0.25$  with a square box ( $\square$ ).

Fig. 9 shows the trade-off that exists between the number of false readings, specifically false positives, and  $\phi$ , the limit of detection for the system for different values of  $\delta$ . The cases solved in the previous section, for  $\delta \leq 0.25$ , are shown as single points because there is no need to consider trade-offs between the sensitivity of the system and the false readings: designs are possible with no false readings for those cases. The

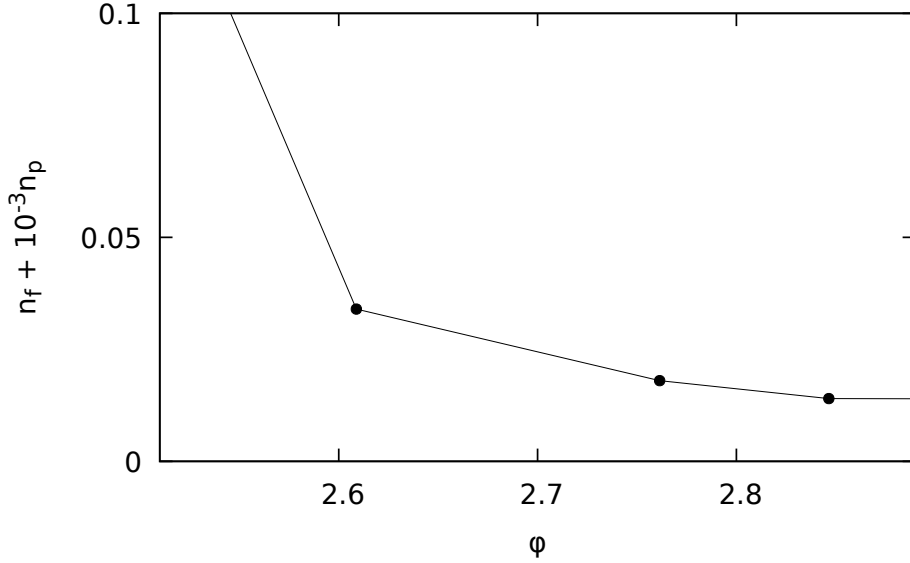


**Figure 10.** Magnified view of the knee of the trade-off curve shown in Fig. 9 for the  $\delta=0.5$  case, highlighting those points which are likely to be of interest for the design of a detector. The lines connecting the points are simply for illustration and do not represent any actual design.

values plotted are the values of  $\phi$  shown in Tables 4 and 5 and with a value of 0 for the second objective indicating a feasible design.

For both graphs in Fig. 9, a point exists lies above and to the left of the leftmost point on the curve shown. This point has been removed as it represents a trivial solution, corresponding to a value of  $\phi=1$ . This value of  $\phi$  leads to a large number of both false negatives and false positives and, hence, corresponds to a design that would not be of any interest for safety reasons.

**Table 6.** Values of the design variables for the designs obtained for different values of the detection interference value,  $\delta$ .

$\delta$	$D$ [mm]	$L_{e_1}$ [m]	$L_s$ [m]	$L_{e_2}$ [m]	$q_{e_1}$	$q_s$	$q_{e_2}$	$\phi$
0.00	0.59	0.15	0.18	0.11	1.28	1.29	1.74	1.45
0.25	0.54	0.05	0.15	0.17	0.64	0.86	0.53	2.30
0.50	0.74	0.22	0.07	0.38	0.50	0.74	0.50	2.76
1.00	0.56	0.22	0.14	0.05	0.50	0.58	0.50	2.62

In the case of  $\delta=0.5$ , the interesting solutions are those in the *knee* of the trade-off curve, shown in a magnified view in Fig. 10. It is likely that the middle point of those shown in this plot would be chosen as the best compromise design. The design values for this solution are presented in row 3 of Table 6. For the top graph, for  $\delta=1.0$ , the cluster of three points towards the left end of the trade-off graph would be of most interest: they have essentially the same number of false positive readings. The design to choose would be that corresponding to the leftmost point; see row 4 of Table 6. This design corresponds to a value of  $\phi=2.6$  approximately. The actual chosen designs for  $\delta=0.5$  and  $\delta=1.0$  are shown graphically in Fig. 11, again using a parallel coordinate system plot.

The results indicate that, should there be significant interference in the signal gener-

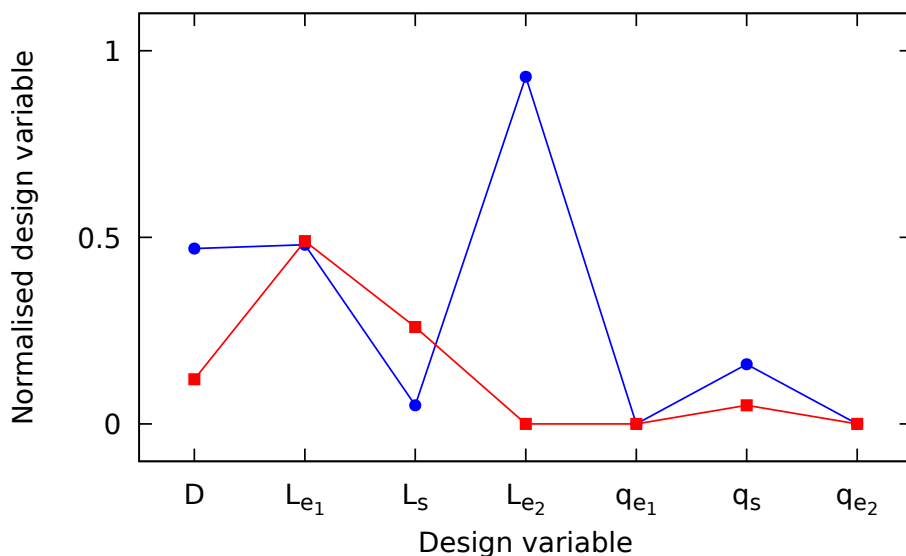


**Figure 11.** Parallel coordinate plot of the design variables for the chosen solutions: in blue with solid circles ( $\bullet$ ) for  $\delta=0.5$  and in red with filled squares ( $\blacksquare$ ) for  $\delta=1.0$ .

ated by the presence of more than one radionuclide, a design that avoids false negative readings with few false positive readings is achievable and one with a limit of detection only three times the actual limits of detection for the particular detection mechanism regardless of the level of interference.

The false positive readings cannot be avoided when there is significant detection interference. This is due to the simple process used for the design of the detection system, allowing for only one extraction step for each radionuclide. To ameliorate the impact of detection interference, a more complex structure would be required. For instance, each single step in the process shown in Fig. 1 could be replaced by a set of steps, maybe with a counter-current configuration to maximise the separation achieved and also minimise the amount of the extractant required. This would enable an increase in the purity of the radionuclides in each of the detection streams and would reduce the number of false positive readings.

## 5. Summary and Conclusions

An optimization based design methodology for the design of a micro-total analysis system for the detection of radionuclides has been presented. A simple process structure, consisting of three process steps, has been considered as the basis of the design. The process structure assumes the use of microchannels, leading to designs that could be implemented on a single wafer. This may lead to availability of inexpensive and easy to manufacture analytic systems.

Each step in the process extracts one radionuclide in preference to the other. As a result, the detector is suitable for the identification of the presence of two different radionuclides. The radionuclides considered here are trivalent lanthanides: Sm and Nd. The process steps take advantage of the difference in distribution coefficients of the two lanthanides. Simulation is used to evaluate each design considered for a large sampling of different feed compositions. During simulation, each step in the process is

a microchannel behaving as a plug flow reactor.

The objective of the optimization based design procedure depends on how well the detection mechanism can differentiate between the different radionuclides. In the case of thermal lens microscopy, there is often some interference in the detection. When the interference is low, a single objective function is defined; when the interference is more significant, a multiple objective formulation is used. In both cases, the aim is to identify the lowest detection limit for the overall detection system that ensures that radionuclides are detected if above this limit. The results have shown that, for this case study, designs for the  $\mu$ TAS using thermal lens microscopy for detection, are obtained with 2-3 times the detection limits imposed by the TLM detection itself.

When the interference in detection is large, the designs obtained will lead to a number of false positive readings: that is, the detector will indicate that a radionuclide may be present in the feed when it is in fact present below the limit of detection. Although the possibility of false positive readings does not compromise safety, it does lead potentially to unnecessary precaution or further analysis of the actual sample fed to the  $\mu$ TAS. Designs that avoid or further minimize false positive readings could be achieved using, for instance, multiple extraction stages for each of the steps in the considered process structure. We have presented the design and optimization methodology for a case study with a two-component system. Where more species may be present, the above methodology would need to be extended to incorporate additional steps with similar structure in the process, assuming of course that the detector itself can differentiate between the species. The unique features of TLM system could be exploited in this case.

The mass transfer models used for simulating the process designs considered do require accurate correlations of the overall mass transfer coefficients. These coefficients are typically developed for standard cases and differ from case to case. An extension of our work could be to find optimum configurations for other reported correlations. Further, in some cases, the distribution coefficient of the radionuclides to be separated may be affected by the concentration of other radionuclides; in this case, the evolution of the concentrations is nonlinear and more complex models may be required. The computational framework caters for sensitivity analysis with respect to the distribution coefficient values and other relevant physical properties of the system. Further investigation will also be required to determine the correlation, if any, between the design parameters and the objective function value,  $\phi$ .

Finally, although we have presented design information for a number of cases, this paper has not considered the layout of the process onto a wafer. Considering the layout may require compromises, depending on the size of the wafer and the lengths of the channels required for separation or extraction. These compromises will naturally lead to multiobjective optimization, possibly trading off the lower detection limit or the number of false positive readings with the size of wafer required. The optimization software used here, Fresa, should be capable of handling the optimization problem defined in these circumstances. From a practical perspective, the implementation of an actual  $\mu$ TAS will require consideration of a number of practical details not taken into account in this computational study. For instance, materials for the microchannels that withstand the radioactivity must be chosen [5,41–44]. Similarly, the sample volumes and the method to pump the liquids into the  $\mu$ TAS must be properly decided. The microfluidic channels make it possible to manipulate nano/microliter liquid volumes for such a  $\mu$ TAS device. Accordingly, a syringe pump and/or airpressure controller can be used to introduce and control the sample solution inside the microchannels.

## ***Acknowledgements***

The authors gratefully acknowledge funding received from UK Research & Innovation through the grant EP/R019223/1 which supported the research presented in this paper. The authors also wish to thank Dr Haoyu Wang, UCL, for use of the photograph in Fig. 3.

## **References**

- [1] Ohno T, Muramatsu Y, Toyama C, et al. Determination of  $^{129}\text{I}$  in Fukushima soil samples by icp-ms with an octopole reaction system. *Anal Sci.* 2013;29:271–4.
- [2] Tomono D, Mizumoto T, Takada A, et al. First on-site true gamma-ray imaging-spectroscopy of contamination near Fukushima plant. *Scientific Reports.* 2017;7:41972.
- [3] Sakamoto T, Morita M, Kanenari K, et al. Isotope-selective microscale imaging of radioactive Cs without isobaric interferences using sputtered neutral mass spectrometry with two-step resonant ionization employing newly-developed Ti:sapphire lasers. *Anal Sci.* 2018;34:1265–1270.
- [4] Haraga T, Ouchi K, Sato Y, et al. Safe and rapid development of capillary electrophoresis for ultratrace uranyl ions in radioactive samples by way of fluorescent probe selection for actinide ions from a chemical library. *Anal Chim Acta.* 2018;1032:188–196.
- [5] Tsukahara T, Hotokezaka H, Harada M, et al. Highly efficient electrochemical valence control of uranium using microfluidic chip equipped with microelectrodes. *Microfluidics and Nanofluidics.* 2013;14:989–994.
- [6] Mawatari K, Kazoe Y, Aota A, et al. Microflow systems for chemical synthesis and analysis: Approaches to full integration of chemical process. *J Flow Chem.* 2012;1:3–12.
- [7] Manz A, Becker H, editors. *Microsystem technology in chemistry and life science.* Berlin: Springer; 1998.
- [8] Haswell SJ, Middleton RJ, OSullivan B, et al. The application of micro reactors to synthetic chemistry. *Chem Commun.* 2001;5:391–398.
- [9] Xu C, Xie T. Review of microfluidic liquid-liquid extractors. *Ind Eng Chem Res.* 2017; 56:7593–7622.
- [10] Sattari-Najafabadi M, Mohsen Nasr Esfahany MN, Wu Z, et al. Mass transfer between phases in microchannels: A review. *Chem Eng Process.* 2018;127:213–237.
- [11] Kashid MN, Gupta A, Renken A, et al. Numbering-up and mass transfer studies of liquid-liquid two phase microstructured reactors. *Chem Eng Sci.* 2010;158:233–240.
- [12] Mariet C, Vansteene A, Losno M, et al. Microfluidic devices applied to radionuclides separation in acidic media for the nuclear fuel cycle. *Micro and Nano Engineering.* 2019; 3:7–14.
- [13] Wang T, Xie T, Xu C. Microextractors applied in nuclear-spent fuel reprocessing: Micro/mini plants and radiochemical analysis. *Crit Rev Environ Sci Technol.* 2019;49:1–31.
- [14] Tsaoulidis D, Angeli P. Effect of channel size on mass transfer during liquid-liquid plug flow in small scale extractors. *Chem Eng Sci.* 2015;15:785–793.
- [15] Li Q, Angeli P. Intensified Eu(III) extraction using ionic liquids in small channels. *Chem Eng Sci.* 2016;143:276–286.
- [16] Bascone D, Angeli P, Fraga ES. A modelling approach for the comparison between intensified extraction in small channels and conventional solvent extraction technologies. *Chem Eng Sci.* 2019;203:201–211.
- [17] Yamamoto M, Taguchi S, Do KV, et al. Development of an online measurement system using an alpha liquid scintillation counter and a glass-based microfluidic solvent extraction device for plutonium analysis. *Appl Radiat Isot.* 2019;152:37–44.
- [18] Do KV, Yamamoto M, Taguchi S, et al. Online coupling of two-phase flow solvent extraction microfluidics with inductively coupled plasma mass spectrometry. *Curr Anal Chem.* 2018;14:111–119.

- [19] Hellé G, Mariet C, Cote G. Liquid-liquid extraction of uranium(vi) with aliquat<sup>®</sup> 336 from hcl media in microfluidic devices: Combination of micro-unit operations and online icp-ms determination. *Talanta*. 2015;139:123–131.
- [20] Uchiyama K, Hibara A, Kimura H, et al. Thermal lens microscope. *Jpn J Appl Phys*. 2000;39:5316–5322.
- [21] Kitamori T, Manabu T, Akihide T, et al. Thermal lens microscope and microchip chemistry. *Anal Chem*. 2004;76:52A–60A.
- [22] Lubej M, Novak U, Mingqiang Liu M, et al. Microfluidic droplet-based liquidliquid extraction: online model validation. *Lab Chip*. 2015;15:2233–2239.
- [23] Gordon JP, Leite RCC, Moore RS, et al. Long transient effects in lasers with inserted liquids samples. *J Appl Phys*. 1965;36:3–8.
- [24] Hotokezaka H, Tokeshi M, Harada M, et al. Development of the innovative nuclide separation system for high-level radioactive waste using microchannel chip extraction behaviour of metal ions from aqueous phase to organic phase in microchannel. *Prog Nucl Energy*. 2005;47:439–447.
- [25] Chen C, Shimizu H, Kitamori T. Review of ultrasensitive readout for micro-/nanofluidic devices by thermal lens microscopy. *J of Optical Microsystems*. 2021;1(2):020901–1.
- [26] Benedict M, Pigford TH, Levi HW, editors. *Nuclear chemical engineering*. 2nd ed. New York (NY): McGrawHill Book Company; 1981.
- [27] Grossmann I, Apap RM, Calfa BA, et al. Recent advances in mathematical programming techniques for the optimisation of process systems under uncertainty. *Comput Chem Eng*. 2016;91:3–14.
- [28] Sahinidis NV. Optimization under uncertainty: state-of-the-art and opportunities. *Comput Chem Eng*. 2004;28:971–983.
- [29] Wannachod T, Leepipatpiboon N, Pancharoen U, et al. Synergistic effect of various neutral donors in d2ehpa for selective neodymium separation from lanthanide series via hfslm. *Journal of Industrial and Engineering Chemistry*. 2014;20(6):4152–4162.
- [30] Yoon SJ, Lee JG, Tajima H, et al. Extraction of lanthanide ions from aqueous solution by bis(2-ethylhexyl)phosphoric acid with room-temperature ionic liquids. *Journal of Industrial and Engineering Chemistry*. 2010;16(3):350–354.
- [31] Shokoufi N, Yoosefian J. Selective determination of Sm(III) in lanthanide mixtures by thermal lens microscopy. *Journal of Industrial and Engineering Chemistry*. 2016;35:153–157.
- [32] Suzuki H, Tsubata Y, Matsumura T, et al. Highly practical and simple ligand for separation of Am(III) and Eu(III) from highly acidic media. *Anal Sci*. 2016;32:477–479.
- [33] Suzuki H, Tsubata Y, Kurosawa T, et al. Continuous extraction and separation of Am(III) and Cm(III) using a highly practical diamide amine extractant. *J Nucl Sci Technol*. 2017;54:1163–1167.
- [34] Suzuki H, Tsubata Y, Matsumura T. High-performance alkyl diamide amine and water-soluble diamide ligand for separation of Am(III) from Cm(III). *Anal Sci*. 2017;33:239–242.
- [35] Bascone D, Angeli P, Fraga ES. Process intensification applied to spent nuclear fuel reprocessing: An alternative flowsheet using small channels. *Chem Eng Process*. 2019;143:107618.
- [36] Dore V, Tsaoulidis D, Angeli P. Mixing patterns in water plugs during water/ionic liquid segmented flow in microchannels. *Chem Eng Sci*. 2012;80:334–341.
- [37] Armbruster D, Pry T. Limit of blank, limit of detection and limit of quantitation. *Clin Biochem Rev*. 2008;29:S49–S52.
- [38] Zhang H, Wang H, Luo X, et al. Toward a mechanistic understanding of microfluidic droplet-based extraction and separation of lanthanides. *Chem Eng Sci*. 2019;356:673–679.
- [39] Zhang H, Wang H, Xu H, et al. Enabling separation intensification of a lanthanide pair with closely similar kinetics based on droplet microfluidics: hydrodynamic and kinetic approaches. *React Chem Eng*. 2019;4:1410–1420.
- [40] Pineda M, Angeli P, Tsukahara T, et al. Devices for analysis of radionuclides. *Comput Aided Chem Eng*. 2019;46:1807–1812.

- [41] Brandt A, Tsukahara T. Development of real-time analysis system of selenium ion in solutions by using microextraction and fluorescence microscopy. *ACS Earth Space Chem.* 2021;5(3):588–595.
- [42] Yamamoto M, Taguchi S, Do VK, et al. Development of an online measurement system using an alpha liquid scintillation counter and a glass-based microfluidic solvent extraction device for plutonium analysis. *Appl Radiat Isot.* 2019;152:37–44.
- [43] Tsukahara T, Ikeda Y. Mutual separation of strontium, cerium, and uranium using pressure-driven flow in 100 nm-sized nanofluidic channels. *Progress in Nuclear Energy.* 2011;53:935–939.
- [44] Ban Y, Kikutani Y, Tokeshi M, et al. Extraction of am(iii) at the interface of organic-aqueous two-layer flow in a microchannel. *J Nucl Sci Technol.* 2011;48:1313–1318.
- [45] Filho PIO, Carmalt CJ, Angeli P, et al. Mathematical modeling for the design and scale-up of a large industrial aerosol-assisted chemical vapor deposition process under uncertainty. *Industrial & Engineering Chemistry Research.* 2020;59(3):1249–1260.
- [46] Fraga ES. The Fresa plant propagation algorithm for optimization; 2021. doi:10.5281/zenodo.5045812; Available from: <http://github.com/ericfraga/Fresa.jl>.
- [47] Salhi A, Fraga ES. Nature-inspired optimisation approaches and the newplant propagation algorithm. In: *Proceedings of the International Conference on Numerical Analysis and Optimisation (ICeMATH2011).*; 2011. p. 1–8.
- [48] Fraga ES. An example of multi-objective optimization for dynamic processes. *Chemical Engineering Transactions.* 2019;74:601–606.
- [49] Bezanson J, Edelman A, Karpinski S, et al. Julia: A fresh approach to numerical computing. *SIAM Rev.* 2017;59(1):65–98.
- [50] Filho PIO, Fraga ES. On the design and implementation of a process modelling language for uncertainty. *Comput Aided Chem Eng.* 2019;46:895–900.
- [51] Garciadiego-Ortega E, Tsaoulidis D, Pineda M, et al. Hydrodynamics and mass transfer in segmented flow small channel contactors for uranium extraction. *Chem Eng Process Process Intensif.* 2020;153:107921.